EurJOC
European Journal of Organic Chemistry

Research Article
doi.org/10.1002/ejoc.202400260

Chemistry Europe
European Chemical Societies Publishing

www.eurjoc.org

Polymorphism and White Light Emission of 1-Bromo-3,5,7-triphenyladamantane Compared with 1,3,5,7-Tetraphenyladamantane

Saravanan Gowrisankar,[a, b] Andrey A. Fokin,[a, c] Jonathan Becker,[d] Neeshma Mathew,[e] Jörn Schmedt auf der Günne,[e] and Peter R. Schreiner*[a, b]

Here we report our investigation of 1-bromo-3,5,7-triphenyladamantane (**1**) and the elucidation of polymorphic crystals (**1 A** and **1 B**) using single crystal X-ray diffraction. In the monoclinic crystal system of **1 A** ($P2_1/n$), we observed CH–π interactions, while Br···Br interactions are absent. Conversely, the Br···Br interactions are an apparent factor in the formation of the monoclinic crystal system of **1 B** ($R\bar{3}$). We compare our findings with 1,3,5,7-tetraphenyladamantane (**2**), characterized by numerous CH–π interactions in the solid. Computational analyses were employed to investigate the interactions within the characteristic dimers present in the unit cells of **1 A** and **1 B**, including visualization of noncovalent interactions and the use of the atoms-in-molecules approach as well as MO analyses. These support the notion of London dispersion (LD) dimer-dimer interactions in **1 A** between the phenyl moieties, whereas **1 B** exhibits additional dimer-dimer Br···Br contacts. In contrast, the crystals of **2** are exclusively held together by CH–π stacking LD interactions, a feature absent in the polymorphs of **1**. Both polymorphic forms of **1** emit white light when subjected to 900 nm continuous wave laser irradiation, displaying a subtle blue shift compared to **2**. The absence of CH–π stacking interactions between the dimers of **1** causes a small red-shift in the emission spectrum.

Polymorphs[1] often exhibit different physical and/or chemical properties that can be important in a number of fields, including pharmaceutical applications,[2] chemical processes,[3] and for preparing new materials (e.g., OLEDs).[4] The number of molecular building blocks available for the crystal engineering of polymorphs increases at an exponential rate.[5] Understanding polymorphism is critical[6] because small changes in molecular packing can result in major changes in, e.g., optical properties,[4c,7] as seen in second harmonic generation (SHG)[8] and third harmonic generation (THG),[9] photoluminescence,[7a,10] and two-photon absorption.[11] Consequently, efforts have been made to control molecular packing for improving properties of organic crystals via chemical functionalization/modifications by means of controlling the crystallization process.[12] As an example, the polymorphism of dipentyl-3,4,9,10-perylendiimide (PDI) was studied recently, and α- and β-phase polymorphs were identified. Only the α-phase exhibits strong SHG due to a non-centrosymmetric unit cell.[13] Polymorphism in substituted bis(squaraine) dyes was shown for polymorphs with entirely different packing structures that also led to large variations in their UV/Vis/NIR absorption properties.[14]

Diamondoid hydrocarbons built only of adamantane repeating units[15] – ultimately forming diamond –, have recently demonstrated nonlinear optical (NLO) properties such as directional white light generation (WLG) and SHG in the solid state upon continuous wave infrared (CW-IR) laser irradiation.[16] In one of our recent studies, we demonstrated a remarkable shift in the nonlinear optical properties of bromophenyl adamantanes, denoted by the general formula $AdBr_xPh_{4-x}$ (x = 0–4). This shift, from SHG to WLG, hinged on the specific number of C–Br bonds present within the molecules. Notably, another interesting possibility emerged during our investigation, namely the potential transition from a crystalline to an amorphous state, induced by laser irradiation.[16b,d] This transition hinted at the possibility of intramolecular structural changes and intermolecular rearrangements within the crystal lattice. We expanded our investigations beyond prior research, delving into the intricacies of molecular packing in these compounds. Our specific

[a] S. Gowrisankar, A. A. Fokin, P. R. Schreiner
Institute of Organic Chemistry Justus Liebig University, 35392 Giessen, Germany
E-mail: prs@uni-giessen.de
Homepage: https://www.uni-giessen.de/schreiner

[b] S. Gowrisankar, P. R. Schreiner
Center for Materials Research, Justus Liebig University Giessen, Heinrich-Buff-Ring 16, 35392 Giessen, Germany

[c] A. A. Fokin
Department of Organic Chemistry, Igor Sikorsky Kiev Polytechnic Institute, Pr. Pobedy 37, 03056 Kiev, Ukraine

[d] J. Becker
Institute of Inorganic and Analytical Chemistry, Justus Liebig University, 35392 Giessen, Germany

[e] N. Mathew, J. Schmedt auf der Günne
University of Siegen, Faculty IV: School of Science and Technology, Department of Chemistry and Biology, Inorganic Materials Chemistry and Center of Micro-and Nanochemistry and Engineering (Cμ), Adolf-Reichwein-Straße 2, 57068 Siegen, Germany

Supporting information for this article is available on the WWW under https://doi.org/10.1002/ejoc.202400260

emphasis was on unravelling the complexities of polymorphism and its impact on nonlinear optical (NLO) properties. An intriguing revelation emerged during our investigation: 1-bromo-3,5,7-triphenyladamantane exhibited a remarkable ability to adopt two distinct crystal structures in the solid state. We chose to thoroughly re-investigate **2** for comparison due to two specific reasons:[16a] Firstly, its striking isomorphism with structures of the general formula XPh_4 (X = C, P, Si, Ge, Sn, Pb), which often display exceptional nonlinear optical properties.[17] Secondly, as previously reported,[18] **2** stands out for its numerous CH–π interactions that arrange the molecules into chains, with both CH (phenyl) and CH_2 (adamantane) groups serving as dispersion energy donors (DEDs).[19]

As mentioned in the introduction, it has been hypothesized that the differences in properties could be attributed to slight variations in intermolecular interactions within the crystal structures. These interactions encompass a wide spectrum, including but not limited to π–π,[20] Br···Br,[21] Br–π,[22] and CH–π[23] interactions. Our research aims to delve deeper into understanding these interactions, providing comprehensive insights into their roles and significance within the context of solid-state behavior and nonlinear optical properties, comparing the polymorphs of **1** with **2** as a reference point for our investigations.

Following the literature protocol, we obtained **1** as a yellow solid and purified it by sublimation.[24] Crystals of **1** were prepared using solvothermal processes, slow solvent evaporation, or fast precipitation; we observed the formation of two polymorphs depending on crystallization technique employed (Scheme 1; for details see the Experimental Section and the SI).[25,16d]

The single-crystal X-ray diffraction data reveal that the crystallization of **1** occurs in two different crystal systems depending on the method employed. When using vapor diffusion, it crystallizes in the monoclinic crystal system ($P2_1/n$) and is denoted as **1 A**. In the crystal structure **1 A** the axial lengths vary along the three axes with the following values: a = 14.7346(5) Å, b = 14.7346(5) Å, and c = 16.5423(6) Å. The angles between these axes are α = 90°, β = 90°, and γ = 120°. On the other hand, the liquid/liquid diffusion method yields the trigonal crystal system ($R\bar{3}$) and is referred to as **1 B** (as illustrated in Scheme 1), with the lengths varying along all axes, and their values are a = 13.1782(8) Å, b = 10.3658(6) Å, and c = 15.3365(10) Å. The angles between these axes are α = 90°, β = 90.641(2)°, and γ = 90°. The sublimation of **1** under argon did not result in crystalline material; instead, a powder formed.[26] Note that no solvent inclusions were detected in either crystal form. For comparison **2**, which generates white light in the amorphous state (*a*-$AdPh_4$) and SHG in the crystalline (*c*-$AdPh_4$) state displays a tetragonal space group ($P\bar{4}2_1c$) with two molecules per unit cell, $Z = 2$. Two of the three axes are equal (a = 12.7632(6) Å, b = 12.7632(6) Å, c = 7.1485(6) Å; α = β = γ = 90°).On the other hand, sublimation of **2** under reduced pressure did not give crystalline material.[24a] No polymorphs were identified upon subjecting this material to a variety of crystallization techniques (*cf.* SI for details). To confirm the absence of polymorphic transitions and to investigate the site disorder, we conducted solid-state nuclear magnetic resonance (NMR) experiments. Thus, we performed a thorough analysis of **2** by specifically conducting $^{13}C(^1H)$ cross-polarization magic-angle-spinning NMR experiments in the solid state (Figure 1) including a determination of anisotropic chemical shift parameters (Table 1) from an analysis of the spinning sideband pattern. Our results indicate that all peaks display a sharp line-shape, with no additional splitting or broadening as expected for static site disorder. Based on these observations, we conclude that the site disorder observed in the diffraction experiments is of dynamic and not static nature. There is no indication of polymorphism either, which would imply additional unassigned peaks (Table 1).

Figure 2 shows a characteristic partial packing view of crystal structures of polymorph **1 A**. In the crystal structure of **1 A** the molecular dipole along the C1—Br direction is oppositely oriented and Br···Br contacts are absent. On the other hand, the solid-state structure of **1 B** displays two characteristic dimeric substructures. The first is virtually identical to the one found in **1 A** (Figure 2) while the other displays a relatively short Br···Br distance of 3.617 Å, which is below the sum of the bromine vdW radii (3.7 Å)[27] and the shortest ever observed in crystals of bromoadamantane derivatives[28a–i,16d,28j,k] (the values vary from 3.724 to 6.923 Å,[29,21b] see Table S1 in SI). Notably, the Br···Br contact distance in 1,3,5,7-tetrabromoadamantane (3.724 Å)[28e] and 1,3,5-tribromo-7-phenyladamantane (3.983 Å)[16d] crystals are significantly longer. Intermolecular Br···Br distances exceeding 4.00 Å were observed for 2-bromoadamantane (5.035 Å),[30] 2-bromotricyclo[3.3.1.1^{3,7}]decane-1-carboxylic acid (4.095 Å),[31]

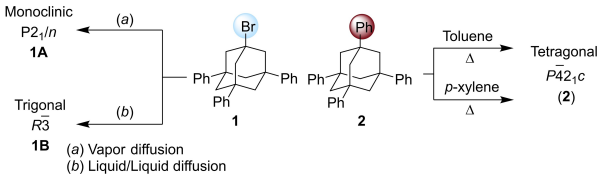

Scheme 1. Crystallization of **1** and **2** depending on conditions.

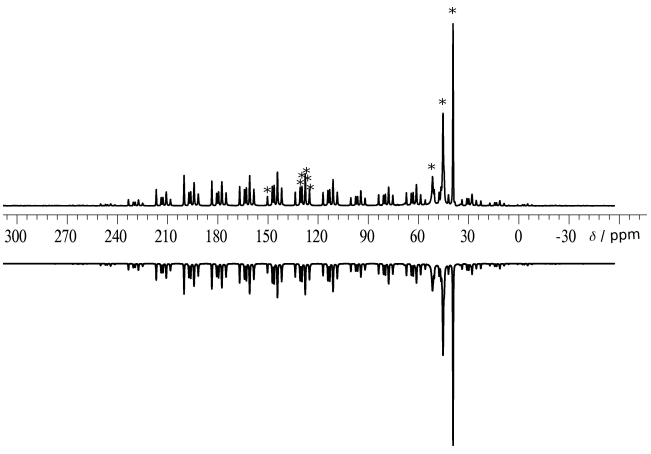

Figure 1. Experimental (top) and simulated (bottom) $^{13}C(^1H)$ ramped CP MAS NMR spectrum of **2** obtained at a spinning frequency of 2.5 kHz; the fit achieved a mean square deviation of 0.14%.

Research Article
doi.org/10.1002/ejoc.202400260

Table 1. The experimental ^{13}C chemical shift parameters for the $AdPh_4$ structure (compound **2**) extracted by non-linear least square fitting of the $^{13}C(^1H)$ CP MAS NMR spectrum (Figure 1).

	Peak A	Peak B	Peak C	Peak D	Peak E	Peak F	Peak G	Peak H	Peak I
δ_{iso}/ppm	148.9	129.5	128.4	126.4	126.4	123.9	50.6	44.3	38.4
δ_{aniso}/ppm	−131	−117	−117	−106	−127	−115	–13	−9	−9
η	0.29	0.79	0.74	0.73	0.74	0.70	0.73	0.54	0.85
δ_{11}/ppm	233	234	230	218	237	221	64	52	47
δ_{22}/ppm	195	142	143	141	143	141	49	47	39
δ_{33}/ppm	18	12	12	20	−1	9	39	35	29
Peak area/a.u.	3.9	4.2	4.0	4.2	4.2	4.4	2.2	4.7	4.5

The isotropic chemical shift δ_{iso}, the anisotropic chemical shift δ_{aniso}, and the asymmetry parameter η are shown; while the eigenvalues δ_{11}, δ_{22}, δ_{33} of the aromatic peaks carry errors of a few ppm, the errors of the atoms in the adamantane cage are bigger because fewer spinning side-bands were available in the experimental line shape. Errors by a non-isotropic excitation profile of the cross-polarization experiment were neglected.

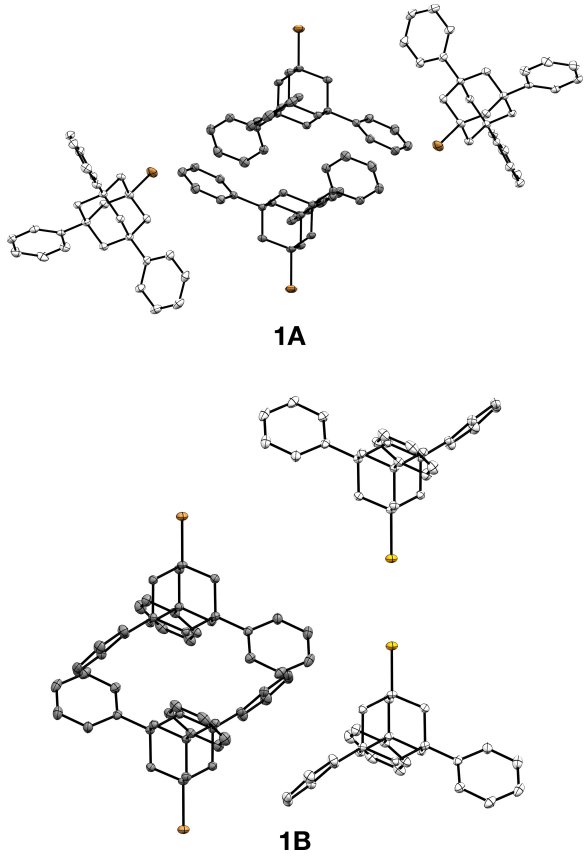

Figure 2. Partial packing view of crystal structures of polymorphs **1 A** and **1 B**. Displacement ellipsoids drawn at the 50% probability level. Hydrogen atoms are omitted for clarity.

1,2,5,6-tetrabromoadamantane (6.530 Å),[28f] and 1,2,3-tribromo-5,7-dimethyladamantane (6.486 Å).[32]

As the unit cell dimer interactions may affect the NLO properties of the crystal[33] the characteristic dimeric fragments of the crystal lattice of **1 AD** ("D" for dimer) and **1 BD**, as well as dimer **2 D** (Figure 3)[18] for comparison, were studied computationally utilizing density functional theory (DFT) at the B3LYP-D3(BJ)/6-31 + G(d,p) level of theory.[34]

Geometry optimizations were performed with Gaussian 16, Revision C.01[35] utilizing the local molecular symmetry observed in the crystals. All optimized structures have only real vibrational frequencies, confirming their nature as minima on the potential energy surface. The optimized geometries were then subjected to natural bond orbital (NBO) analysis[36] at the B3LYP)/aug-cc-pVTZ//B3LYP-D3(BJ)/6-31 + G(d,p) level of theory. DLPNO-CCSD(T)/cc-pVTZ[37] single point energy computations on the B3LYP-D3(BJ)/6-31 + G(d,p) optimized geometries using the ORCA program[38] were performed to obtain more reliable dimerization energies. Bond critical points were localized utilizing Atom-in-Molecules[39] computations with the AIMALL program.[40] The S_6-point group optimized geometries of **1 AD** and **1 BD** agree well with experiment as the computed key interatomic distance values differ only within ±0.2 Å as compared to the X-ray data (Figure 4, left).

The nature of the bonding in **1 AD** and **1 BD** is clearly different. While only very weak Br···Br bonding is present in **1 BD**, **1 AD** is effectively stabilized by noncovalent interactions (NCI) between six phenyl moieties. The noncovalent interaction (NCI)[41] plots (Figure 4, right), displayed as green isosurfaces accounting predominantly for attractive LD interactions, are responsible for the bonding in **1 AD**. This finding is supported by the shortest H···H contact distances in **1 AD** (ca. 2.2 Å) that are below the sum of the hydrogen vdW-radii (2.4 Å). As a consequence, **1 AD** is characterized by a large association energy of 26.8 kcal mol^{-1} [DLPNO-CCSD(T)/cc-pVTZ//B3LYP-D3(BJ)/6-31 + G(d,p)] and this substructure is present in both **1 A** and **1 B**, while weakly bonded **1 BD** [the computed dissociation energy is 2.7 kcal mol^{-1} at B3LYP-D3(BJ)/6-31 + G(d,p)] and 0.1 kcal mol^{-1} at DLPNO-CCSD(T)/cc-pVTZ//B3LYP-D3(BJ)/6-31 + G(d,p)] is present only in **1 B**. Note that despite such a low dissociation energy the AIM analysis indicates a bond critical point between the bromine atoms in **1 BD** (Figure 5).

The shapes of the highest occupied (HOMO) and lowest unoccupied (LUMO) molecular orbitals of the dimers are shown in Figure 6. Both **1 AD** and **1 BD** HOMOs describe CC bonding in phenyl groups, but doubly degenerate HOMO of **1 BD** additionally involves the antibonding between the bromine lone pairs.

Research Article
doi.org/10.1002/ejoc.202400260

Chemistry Europe
European Chemical Societies Publishing

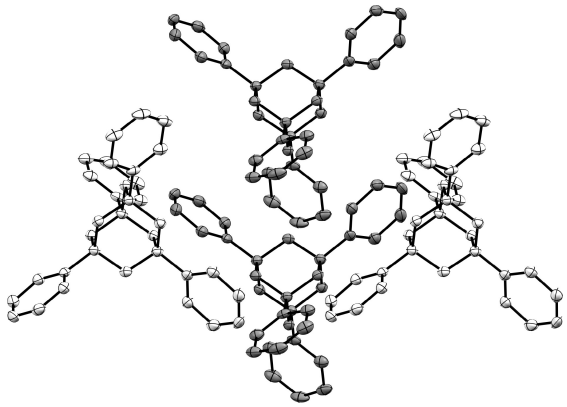

2

Figure 3. Partial packing view of crystal structures of **2** to represent **2 D**. Displacement ellipsoids drawn at the 50% probability level. Hydrogen atoms are omitted for clarity.

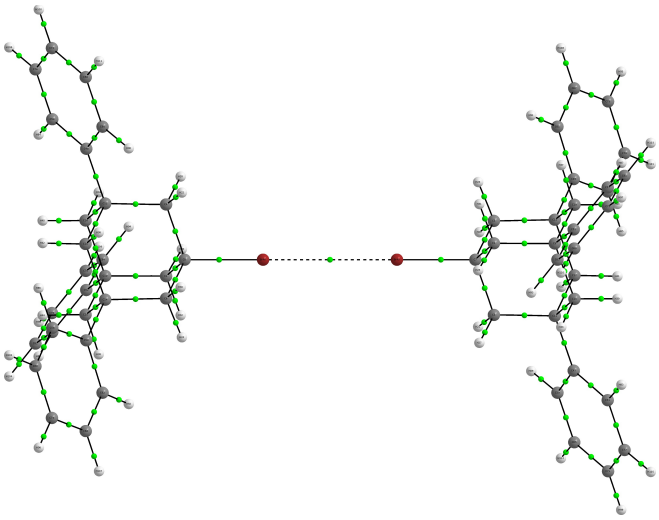

Figure 5. Bond critical points (in green) in **1 BD** based on AIM computations using the B3LYP-D3(BJ)/6-31 + G(d,p) optimized structure (ring critical points are omitted for clarity).

In contrast, the LUMOs of **1 AD** and **1 BD** differ in nature as the LUMO of **1 AD** describes the CC antibonding in the phenyl moieties, whereas the intermolecular Br···Br bonding dominates in the LUMO of **1 BD**. While the HOMO-LUMO energy separation in **1 AD** and **1 BD** are similar (ca. 6 eV (Table 2)) intermolecular binding in the **1 BD** dimer should facilitate electron transfer within the **1 B** crystal lattice via the Br···Br bridge if the LUMO is involved.

From this viewpoint, the structure of **2 D** is instructive because, although the HOMO-LUMO gap is similar to **1D** the packing mode in **2** is clearly different and arises from local molecular symmetries of **1** and **2**: While the C_3-axial symmetry

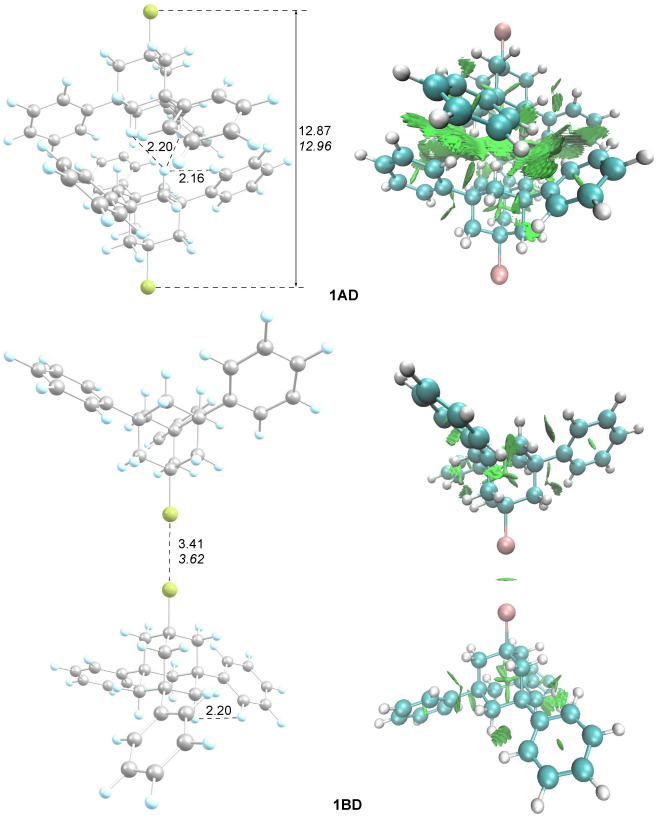

Figure 4. Left: B3LYP-D3(BJ)/6-31 + G(d,p) optimized structures of **1 AD** and **1 BD**, re-optimized starting from the polymorphs **1 A** and **1 B** (key interatomic distances in Å, experimental values in italics). Right: Noncovalent attraction isosurfaces (NCI); the green areas indicate van-der-Waals interactions, in particular LD.

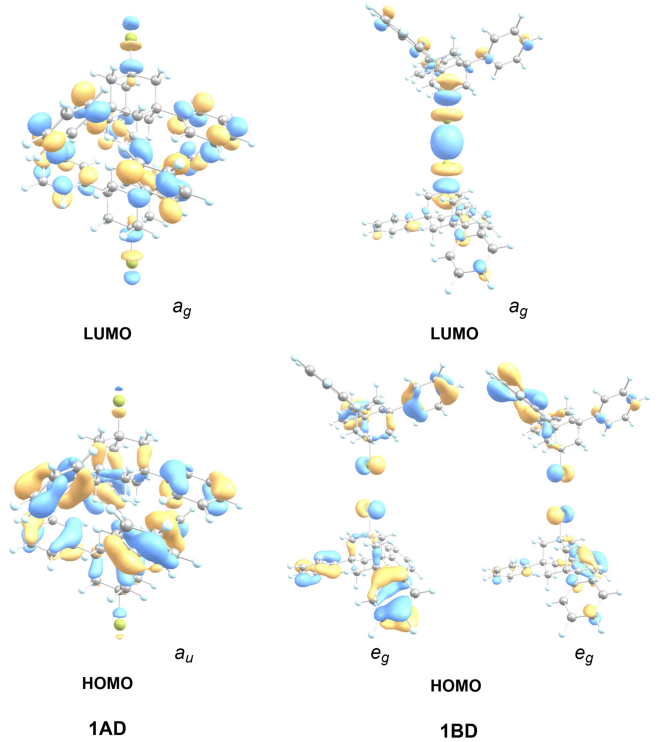

Figure 6. The shapes and symmetries of the HOMOs and LUMOs of **1 AD** and **1 BD** computed at the B3LYP/aug-cc-pVTZ//B3LYP-D3(BJ)/6-31 + G(d,p) level of theory (cf. Table 1).

Research Article
doi.org/10.1002/ejoc.202400260

Table 2. The frontier orbitals characteristics[a] of **1 AD**, **1 BD**, and **2 D**.

Structure	ΔE_{HL} (*eV*)[a]	PG[b]	SG[bc]	HOMO	LUMO
1 AD	5.89	S_6	$P2_1/n$	a_u	a_g
1 BD	5.86	S_6	$R\bar{3}$	e_g	a_g
2 D	5.85	S_4	$P\bar{4}2_1c$	e	b

[a]HOMO-LUMO energy separation at B3LYP/aug-cc-pVTZ//B3LYP-D3(BJ)/6-31 + G(d,p). [b]PG = Point group [c]SG = Space group.

of **1** allows the formation of LD-stabilized dimers involving all phenyl moieties (like in **1 AD**) only a C_2-axis is present in **2** (overall point group S_4). This determines the packing in the crystal whilst retaining the local dimer symmetry in the unit cell (Figure 6).

Remarkably, the dimeric unit cell of **2 D** is almost perfectly constructed as the shortest observed H···H-contact is close to the optimal hydrogen vdW distance (2.4 Å), with the adamantane cages and phenyl groups both being involved in LD interactions. Strong LD attraction between the constituents can be seen from the NCI plots of **2 D** (Figure 7, right) and this parallels its high association energy of 20.4 kcal mol^{-1} at DLPNO-CCSD(T)/cc-pVTZ//B3LYP-D3(BJ)/6-31 + G(d,p), which, however, is smaller than that of slightly polar **1 AD**. This is in accord with the number of interacting phenyl groups in **1 AD** and **2 D** (four and six, respectively). The S_4 symmetry of **2 D** allows almost perfect CH–π LD stacking interactions between the dimers within the crystal cell with formation of linear aggregates. Such a packing motif is a key factor,[42] which may determine the optical properties of **2** in the crystalline form. This clearly is not the case for **1 A** and **1 B**, where CH–π stacking interactions between the dimers are not observed in the crystal unit cell.

We calculated the crystallite (grain) size of **1 A**, **1 B**, and **2** using PXRD data (Figure 8) by determining the average crystal size through the full width at half maximum (FWHM) and Scherrer's equation.[43] In our case, these calculations suggested nm-sized crystals falling within the range of 28–50 nm (**1 A**), 26–45 nm (**1 B**), and 5–37 nm (**2**). Secondly, we notice – and this is a key condition for WLG – that the polymorphs do show slightly different PXRD patterns: While the signal positions are virtually identical, the relative peak intensities differ noticeably.

Finally, we delved into the nonlinear optical properties of **1 A**, **1 B**, and **2**. We employed a continuous-wave diode laser with a central wavelength of 900 nm for excitation. To ensure precision, the samples were maintained under high-vacuum conditions during laser irradiation.

Compounds **1 A** and **1 B** produced WLG starting at 491 nm (2.52 eV) upon 900 nm continuous wave laser irradiation at 728 mW, as shown in the photopic spectra in Figure 9a. When the laser power was reduced to 630 mW, no WLG was observed. Notably, the emission displayed a small but noticeable blue shift when comparing **1 A** and **1 B** to **2**. Specifically, **1 A** exhibited a difference of 8 nm, while **1 B** showed a difference of

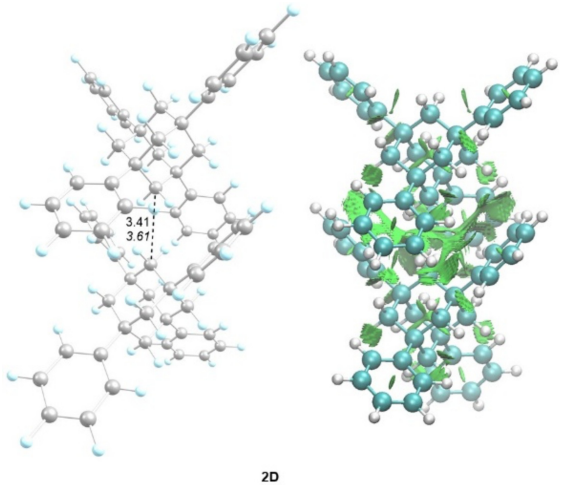

Figure 7. *Left*: B3LYP-D3(BJ)/6-31 + G(d,p) optimized structure of **2 D** (key interatomic distances in Å, X-ray crystal structure analysis values in italics). *Right*: The NCI isosurfaces in **2 D**.

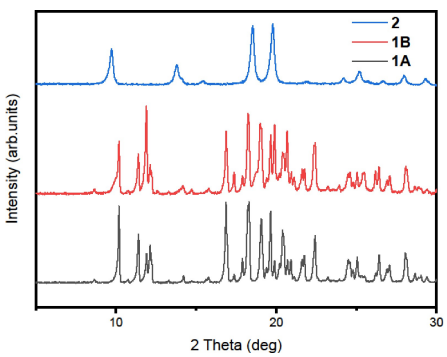

Figure 8. Powder X-ray diffraction patterns of **1 A**, **1 B**, and **2**.

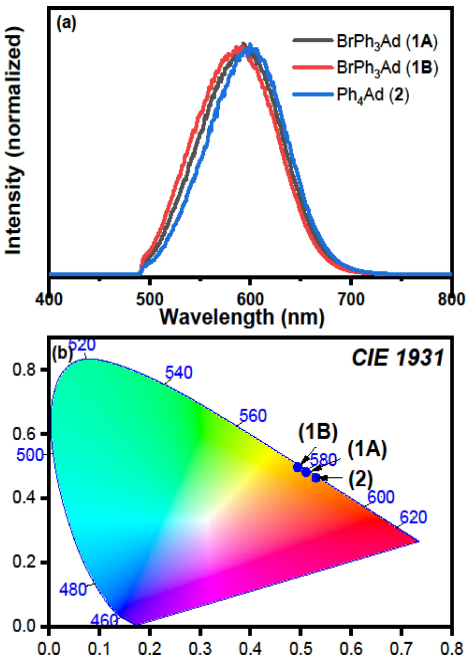

Figure 9. Photopic white-light spectra of (a) **1 A**, **1 B**, and **2**. All spectra were obtained upon irradiation with a 980 nm laser at a power output of 728 mW. (b) Color points in the CIE 1931 chromaticity diagram shows yellowish-red.

14 nm when compared to **2**. This change in emission may be attributed to the absence of inter-dimer CH–π interactions in both **1 A** and **1 B**. Most importantly, the WLG emissions for the polymorphs are different, even in their partially amorphized state.

To provide a better visualization of the white-light color impression, the emitted spectrum is shown as it is perceived by the human eye under photopic vision (converted under use of the 1931 CIE photopic luminosity function) (Figure 9b). In this depiction, it becomes clear that the emitted spectrum covers the whole visible range and peaks at ≈580 nm in radiometric representation, the emission of all samples rises monotonously toward the yellowish-red part of the spectrum. Thus, the emitted light is warm-white.

In summary, our study focuses on the polymorphism of 1-bromo-3,5,7-triphenyladamantane (**1**) in comparison with 1,3,5,7-tetraphenyladamantane (**2**), with specific emphasis on their nonlinear optical properties. Employing a variety of crystallization techniques, we successfully obtained two distinct polymorphs of **1**, namely the monoclinic form (**1 A**) and the trigonal form (**1 B**). In the crystal structure of **1 A**, the primary forces governing molecular assembly are LD attractions, particularly between the phenyl moieties within dimer **1 AD**. We uncovered the dimer **1 BD** substructure in polymorph **1 B**, characterized by faint but discernible Br···Br contacts. In contrast, the crystals of **2** are mostly stabilized by CH–π LD stacking interactions, not only within the dimers but also throughout the linear aggregates in the unit cell – a feature absent in the polymorphs of **1**. These differences in intermolecular interactions likely contribute to the observed variations in nonlinear optical properties between these compounds.

Experimental Section

All the reagents were obtained from commercial suppliers and used without further purification. The flask was flushed under argon and well stoppered.

Crystallization of 1-bromo-3,5,7-triphenyladamantane (1 A): Standard air-exclusive techniques were utilized to prepare a solution containing the **1** (25 mg) in DCM. These techniques encompassed the use of dry solvents, evacuation, and inert gas refilling in the first flask before use. Hexane was then added to the second Schlenk flask and allowed to diffuse into the first flask through a U-junction adapter. After a week, a crystal suitable for X-ray diffraction analysis was successfully obtained.

Crystallization of 1-bromo-3,5,7-triphenyladamantane (1 B): **1** was dissolved in DCM, serving as the first solvent in the Schlenk flask's bottom layer. Hexane, the second solvent, was added cautiously and gradually atop the first solvent to ensure a clear and distinct liquid-liquid boundary. This gradual solvent diffusion, led to a progressive decrease in solubility and, ideally, the growth of high-quality crystals. It took approximately one week to obtain a crystal of the polymorph **1 B** suitable for X-ray diffraction analysis.

Solid State NMR: $^{13}C(^{1}H)$ ramped Cross Polarization Magic Angle Spinning (CP MAS) solid state experiments were performed at 14.1 T on a Bruker Avance Neo spectrometer with a commercial 3.2 mm MAS probehead at a frequency of 600.2 for ^{1}H and 150.9 MHz for ^{13}C, respectively. The ^{1}H resonance of 1% TMS in $CDCl_3$ served as an external secondary reference using the Ξ values for ^{13}C as reported by IUPAC.[44] The $^{13}C(^{1}H)$ ramped CP MAS NMR was acquired at a low spinning frequency of 2.5 kHz. The contact time used was 1000 μs and the TPPM-15[45] sequence was used at a decoupling power of 82 kHz for ^{1}H decoupling. For deconvolution and fitting of spectra, the program deconv2Dxy[46] and SIMPSON package (version simpson-4.2.3)[47] were used. The isotropic chemical shift δ_{iso}, the anisotropic chemical shift δ_{aniso} and the asymmetry parameter η were extracted using the SIMPSON package in combination with home written fitting packages and follow the definitions as specified in the original simpson article.[47b]

Measurement of the Nonlinear Optical Response: For excitation a CW Solid-state Laser-diode (Roithner RTLMDL-980-1W) with a wavelength of 980 nm was used. Measurements were performed with a maximum power of 728 mW at the sample position. The excitation laser was attenuated with various reflective neutral density filters. The samples were placed in a small vacuum cell equipped with glass windows and kept at a pressure below 10^{-1} mbar. The vacuum cell was situated under a custom build confocal microscope with a 4x objective (Olympus RMS4X). The light from the sample was separated from the laser with a dichroic mirror (Thorlabs DMLP900R) and focussed onto the face of an optical fiber leading to the spectrometer using a silver-coated off-axis parabolic mirror. A dielectric short pass filter (Thorlabs FESH900) was placed in front of the fiber, to further attenuate the fundamental laser line. The light was then detected using a miniature spectrometer with integrated grating (OceanOptics USB650, 350–1000 nm).

Powder X-Ray Diffraction: Powder X-ray diffraction data for **1 A** and **1 B** were collected on a STOE STADI P equipped with a Dectris Mythen 1 K detector in Debye-Scherrer geometry. All data were collected using Cu–Kα radiation with wavelength 1.54178 Å.

Crystallographic data: The details of the X-ray analyses are described in the Supporting Information. Deposition Numbers 2252951 (for **1 A**), and 2252952 (for **1 B**) contain the supplementary crystallographic data for this paper. These data are provided free of charge by the joint Cambridge Crystallographic Data Centre.

Supporting Information

All details regarding experimental and crystal structures are provided in the Supporting Information. The original spectroscopic and additional data have been deposited at https://doi.org/10.22029/jlupub-18425

Acknowledgements

This work was supported by the Deutsche Forschungsgemeinschaft within the framework of FOR 2824 (SCHR 597/37-2). The authors express their gratitude to Dr. Dennis Gerbig for assisting with the AIM computations. Open Access funding enabled and organized by Projekt DEAL.

Conflict of Interests

The authors declare no conflict of interest.

Data Availability Statement

The data that support the findings of this study are openly available in JLUpub at https://dx.doi.org/10.22029/jlupub-18425, reference number 18425.

Keywords: Bromoadamantane · Br···Br interaction · Crystallization · Polymorphs · White-light generation

[1] a) J. Bernstein, *Polymorphism in Molecular Crystals*., Clarendon Press, 2002; b) J. D. Dunitz, J. Bernstein, *Acc. Chem. Res.* **1995**, *28*, 193–200; c) R. J. Davey, *Chem. Commun.* **2003**, 1463–1467; d) J. Steed, *Acta Crystallogr. Sect. B* **2016**, *72*, 805–806.

[2] a) C. Ouvrard, S. L. Price, *Cryst. Growth Des.* **2004**, *4*, 1119–1127; b) P. Vishweshwar, J. A. McMahon, M. Oliveira, M. L. Peterson, M. J. Zaworotko, *J. Am. Chem. Soc.* **2005**, *127*, 16802–16803; c) S. M. Guthrie, D.-M. Smilgies, G. Giri, *Cryst. Growth Des.* **2018**, *18*, 602–606; d) D. Chistyakov, G. Sergeev, *Pharmaceutica* **2020**, *12*, 34; e) C. I. Sainz-Díaz, A. P. de la Luz, C. Barrientos-Salcedo, M. Francisco-Márquez, C. Soriano-Correa, *J. Comput.-Aided Mol. Des.* **2022**, *36*, 549–562.

[3] a) A. Y. Lee, D. Erdemir, A. S. Myerson, *Annu. Rev. Chem. Biomol. Eng.* **2011**, *2*, 259–280; b) T.-T. C. Lai, J. Cornevin, S. Ferguson, N. Li, B. L. Trout, A. S. Myerson, *Cryst. Growth Des.* **2015**, *15*, 3374–3382; c) T. B. Hansen, E. Simone, Z. Nagy, H. Qu, *Org. Process Res. Dev.* **2017**, *21*, 855–865; d) P. M. Piaggi, M. Parrinello, *Proc. Natl. Acad. Sci. USA* **2018**, *115*, 10251–10256; e) Y. Gui, C. Huang, C. Shi, T. Stelzer, G. G. Z. Zhang, L. Yu, *J. Chem. Phys.* **2022**, *156*, 144504–144515.

[4] a) H. D. Keith, *Macromolecules* **1982**, *15*, 114–122; b) D. A. Safin, K. Robeyns, M. G. Babashkina, Y. Filinchuk, A. Rotaru, C. Jureschi, M. P. Mitoraj, J. Hooper, M. Brela, Y. Garcia, *CrystEngComm* **2016**, *18*, 7249–7259; c) C. Li, Z. Gao, P. Zhao, X. Tian, H. Wang, Q. Wu, W. Lu, Y. Sun, D. Cui, X. Tao, *Cryst. Growth Des.* **2019**, *19*, 1767–1777; d) L. Huang, Q. Wang, F. He, X. Liu, Z. Chen, W. He, X. Luo, D. Gao, J. Bi, G. Zou, *J. Alloys Compd.* **2019**, *771*, 547–554; e) T. Salzillo, A. Brillante, *Adv. Mater. Interfaces* **2022**, *9*, 2200815.

[5] a) D. Braga, J. Bernstein, in *Making Crystals by Design*, **2006**, pp. 293–314 Wiley-VCH, Weinheim; b) A. J. Cairns, J. A. Perman, L. Wojtas, V. C. Kravtsov, M. H. Alkordi, M. Eddaoudi, M. J. Zaworotko, *J. Am. Chem. Soc.* **2008**, *130*, 1560–1561; c) T. A. Maula, H. W. Hatch, V. K. Shen, S. Rangarajan, J. Mittal, *Mol. Syst. Des. Eng.* **2019**, *4*, 644–653; d) M. K. Corpinot, D.-K. Bučar, *Cryst. Growth Des.* **2019**, *19*, 1426–1453.

[6] a) W. MacCrone, Interscience, New York, **1965**; b) J. Bernstein, *Polymorphism in Molecular Crystals 2e, Vol. 30*, International Union of Crystal, **2020**.

[7] a) M. Li, A. H. Balawi, P. J. Leenaers, L. Ning, G. H. L. Heintges, T. Marszalek, W. Pisula, M. M. Wienk, S. C. J. Meskers, Y. Yi, F. Laquai, R. A. J. Janssen, *Nat. Commun.* **2019**, *10*, 2867; b) P. Netzsch, F. Pielnhofer, R. Glaum, H. A. Höppe, *Chem. Eur. J.* **2020**, *26*, 14745–14753.

[8] a) S. J. Ewing, D. I. Woodward, A. V. Powell, P. Vaqueiro, *J. Solid State Chem.* **2013**, *204*, 159–165; b) A. Cammarata, W. Zhang, P. S. Halasyamani, J. M. Rondinelli, *Chem. Mater.* **2014**, *26*, 5773–5781; c) Y. Yang, K. Wu, B. Zhang, X. Wu, M.-H. Lee, *Chem. Mater.* **2020**, *32*, 1281–1287; d) T. Baiheti, S. Han, A. Tudi, Z. Yang, S. Pan, *J. Mater. Chem. C* **2020**, *8*, 11441–11448; e) S. Sundareswaran, S. Karuppannan, *Opt. Laser Technol.* **2021**, *134*, 106667.

[9] a) S.-Y. Hong, J. I. Dadap, N. Petrone, P.-C. Yeh, J. Hone, R. M. Osgood, *Phys. Rev. X* **2013**, *3*, 021014; b) S. Semin, X. Li, Y. Duan, T. Rasing, *Adv. Opt. Mater.* **2021**, *9*, 2100327.

[10] a) A. Moliterni, D. Altamura, R. Lassandro, V. Olieric, G. Ferri, F. Cardarelli, A. Camposeo, D. Pisignano, J. E. Anthony, C. Giannini, *Acta Crystallogr. Sect. B* **2020**, *76*, 427–435; b) C. Carayon, C. André-Barrès, N. Leygue, N. Saffon-Merceron, M. Boggio-Pasqua, S. Fery-Forgues, *Dyes Pigm.* **2021**, *187*, 109119.

[11] a) I. F. A. Mariz, S. Raja, T. Silva, S. Almeida, É. Torres, C. Baleizão, E. Maçôas, *Dyes Pigm.* **2021**, *193*, 109470; b) X. Zhang, J. De, H. Liu, Q. Liao, S.-T. Zhang, C. Zhou, H. Fu, B. Yang, *Adv. Opt. Mater.* **2022**, *10*, 2200286.

[12] a) C. Park, J. E. Park, H. C. Choi, *Acc. Chem. Res.* **2014**, *47*, 2353–2364; b) P. Yu, Y. Zhen, H. Dong, W. Hu, *Chem* **2019**, *5*, 2814–2853; c) M. Li, C. Zhang, M. Li, F. Liu, L. Zhou, Z. Gao, J. Sun, D. Han, J. Gong, *Chem. Eng. J.* **2022**, *429*, 132450.

[13] F. Marin, S. Tombolesi, T. Salzillo, O. Yaffe, L. Maini, *J. Mater. Chem. C* **2022**, *10*, 8089–8100.

[14] C.-A. Shen, D. Bialas, M. Hecht, V. Stepanenko, K. Sugiyasu, F. Würthner, *Angew. Chem. Int. Ed.* **2021**, *60*, 11949–11958.

[15] a) H. Schwertfeger, A. A. Fokin, P. R. Schreiner, *Angew. Chem. Int. Ed.* **2008**, *47*, 1022–1036; b) M. A. Gunawan, J.-C. Hierso, D. Poinsot, A. A. Fokin, N. A. Fokina, B. A. Tkachenko, P. R. Schreiner, *New J. Chem.* **2014**, *38*, 28–41; c) M. A. Gunawan, D. Poinsot, B. Domenichini, P. R. Schreiner, A. A. Fokin, J.-C. Hierso, in *Chemistry of Organo-Hybrids*, (Eds.: B. Charleux, C. Copéret, E. Lacôte), John Wiley & Sons, Hoboken ed., **2014**, pp. 69–113.

[16] a) N. W. Rosemann, H. Locke, P. R. Schreiner, S. Chatterjee, *Adv. Opt. Mater.* **2018**, *6*, 1701162; b) S. Dehnen, P. R. Schreiner, S. Chatterjee, K. Volz, N. W. Rosemann, W.-C. Pilgrim, D. Mollenhauer, S. Sanna, *ChemPhotoChem* **2021**, *5*, 1033–1041; c) S. Gowrisankar, B. Bernhardt, J. Becker, P. R. Schreiner, *Eur. J. Org. Chem.* **2021**, 6806–6810; d) J. Belz, J. Haust, M. J. Müller, K. Eberheim, S. Schwan, S. Gowrisankar, F. Hüppe, A. Beyer, P. R. Schreiner, D. Mollenhauer, S. Sanna, S. Chatterjee, K. Volz, *J. Phys. Chem. C* **2022**, *126*, 9843–9854; e) M. J. Müller, F. Ziese, J. Belz, F. Hüppe, S. Gowrisankar, B. Bernhardt, S. Schwan, D. Mollenhauer, P. R. Schreiner, K. Volz, S. Sanna, S. Chatterjee, *Opt. Mater. Express* **2022**, *12*, 3517–3529.

[17] a) M. A. Lloyd, C. P. Brock, *Acta Crystallogr. Sect. B* **1997**, *53*, 780–786; b) T. Lin, X.-M. Liu, C. He, *J. Phys. Chem. B* **2004**, *108*, 17361–17368; c) R. L. Gieseking, T. R. Ensley, H. Hu, D. J. Hagan, C. Risko, E. W. Van Stryland, J.-L. Brédas, *J. Am. Chem. Soc.* **2015**, *137*, 9635–9642; d) K. Eberheim, C. Dues, C. Attaccalite, M. J. Müller, S. Schwan, D. Mollenhauer, S. Chatterjee, S. Sanna, *J. Phys. Chem. C* **2022**, *126*, 3713–3726.

[18] I. Boldog, A. B. Lysenko, E. B. Rusanov, A. N. Chernega, K. V. Domasevitch, *Acta Crystallogr. Sect. C* **2009**, *65*, o248–o252.

[19] S. Grimme, R. Huenerbein, S. Ehrlich, *ChemPhysChem* **2011**, *12*, 1258–1261.

[20] G. Barin, A. Coskun, M. M. G. Fouda, J. F. Stoddart, *ChemPlusChem* **2012**, *77*, 159–185.

[21] a) H. Li, Y. Lu, Y. Liu, X. Zhu, H. Liu, W. Zhu, *Phys. Chem. Chem. Phys.* **2012**, *14*, 9948–9955; b) G. Cavallo, P. Metrangolo, R. Milani, T. Pilati, A. Priimagi, G. Resnati, G. Terraneo, *Chem. Rev.* **2016**, *116*, 2478–2601.

[22] a) A. N. M. M. Rahman, R. Bishop, D. C. Craig, M. L. Scudder, *CrystEngComm* **2003**, *5*, 422–428; b) A. S. Paton, A. J. Lough, T. P. Bender, *CrystEngComm* **2011**, *13*, 3653–3656; c) S. Yamada, *Chem. Rev.* **2018**, *118*, 11353–11432; d) C. Heroven, V. Georgi, G. K. Ganotra, P. Brennan, F. Wolfreys, R. C. Wade, A. E. Fernández-Montalván, A. Chaikuad, S. Knapp, *Angew. Chem. Int. Ed.* **2018**, *57*, 7220–7224.

[23] a) C. Qin, Q. Yuan, P. Li, S. Wang, S. Chen, M. Zhu, *RSC Adv.* **2020**, *10*, 11493–11498; b) N. Kishida, Y. Tanaka, M. Yoshizawa, *Chem. Eur. J.* **2022**, *28*, e202202075; c) K. M. Herman, E. Aprà, S. S. Xantheas, *Phys. Chem. Chem. Phys.* **2023**, *25*, 4824–4838.

[24] a) H. Newman, *Synthesis* **1972**, 692–693 ; b) A. A. Fokin, P. R. Schreiner, *Adv. Synth. Catal.* **2003**, *345*, 1035–1052; c) K. Nasr, N. Pannier, J. V. Frangioni, W. Maison, *J. Org. Chem.* **2008**, *73*, 1056–1060.

[25] M. Kitamura, *CrystEngComm* **2009**, *11*, 949–964.

[26] a) V. N. Emel'yanenko, R. N. Nagrimanov, B. N. Solomonov, S. P. Verevkin, *J. Chem. Thermodyn.* **2016**, *101*, 130–138; b) G. L. Perlovich, T. V. Volkova, *Phys. Chem. Chem. Phys.* **2018**, *20*, 19784–19791.

[27] a) R. S. Rowland, R. Taylor, *J. Phys. Chem.* **1996**, *100*, 7384–7391; b) S. S. Batsanov, *Inorg. Mater.* **2001**, *37*, 871–885.

[28] a) J. J. Sosnowski, A. L. Rheingold, R. K. Murray Jr., *J. Org. Chem.* **1985**, *50*, 3788–3791; b) W.-S. Chung, Y.-D. Liu, N.-J. Wang, *J. Chem. Soc. Perkin Trans. 2* **1995**, 581–586 ; c) P. R. Schreiner, A. A. Fokin, O. Lauenstein, Y. Okamoto, T. Wakita, C. Rinderspacher, G. H. Robinson, J. K. Vohs, C. F. Campana, *J. Am. Chem. Soc.* **2002**, *124*, 13348–13349; d) R. Betz, P. Klufers, P. Mayer, *Acta Crystallogr. Sect. E* **2009**, *65*, o101; e) Y.-M. Zhang, C. Cao, Y.-Y. Lu, Q.-S. Zhang, T.-B. Wei, *Acta Crystallogr. Sect. E* **2011**, *67*, o286; f) X. Wang, Y. Dong, E. L. Ezell, J. C. Garrison, J. K. Wood, J. P. Hagen, J. L. Vennerstrom, *Tetrahedron* **2017**, *73*, 2972–2976; g) S. Mohamed, L. Li, *CrystEngComm* **2018**, *20*, 6026–6039; h) P. Negrier, B. Ben Hassine, M. Barrio, M. Romanini, D. Mondieig, J.-L. Tamarit, *CrystEngComm* **2020**, *22*, 1230–1238; i) A. Aznar, P. Negrier, A. Planes, L. Mañosa, E. Stern-Taulats, X. Moya, M. Barrio, J.-L. Tamarit, P. Lloveras, *Appl. Mater. Today* **2021**, *23*, 101023; j) M. Bhakat, B. Khatua, J. Guin, *Org. Lett.* **2022**, *24*, 5276–5280; k) L. Xu, Y. Zhang, H.-H. Jiang, N. Zhang, R.-G. Xiong, H.-Y. Zhang, *Adv. Sci.* **2022**, *9*, 2201702.

[29] a) Y. Shimoikeda, M. Machida, *J. Korean Phys. Soc.* **1999**, *35*, S1423–S1425; b) W. Guo, E. Galoppini, R. Gilardi, G. I. Rydja, Y.-H. Chen, *Cryst. Growth Des.* **2001**, *1*, 231–237.

[30] P. Negrier, M. Barrio, J. L. Tamarit, D. Mondieig, *J. Phys. Chem. B* **2014**, *118*, 9595–9603.
[31] M. Larrosa, B. Zonker, J. Volkmann, F. Wech, C. Logemann, H. Hausmann, R. Hrdina, *Chem. Eur. J.* **2018**, *24*, 6269–6276.
[32] E. A. Ivleva, E. V. Simatova, M. S. Zaborskaya, M. S. Kazachkova, V. B. Rybakov, Y. N. Klimochkin, *Russ. J. Org. Chem.* **2023**, *59*, 409–416.
[33] S. Schwan, A. J. Achazi, F. Ziese, P. R. Schreiner, K. Volz, S. Dehnen, S. Sanna, D. Mollenhauer, *J. Comput. Chem.* **2023**, *44*, 843–856.
[34] a) A. D. Becke, *J. Chem. Phys.* **1988**, *88*, 1053–1062; b) C. Lee, W. Yang, R. G. Parr, *Phys. Rev. B Condens. Matter* **1988**, *37*, 785–789; c) S. Grimme, S. Ehrlich, L. Goerigk, *J. Comput. Chem.* **2011**, *32*, 1456–1465.
[35] M. J. Frisch, G. W. Trucks, H. B. Schlegel, G. E. Scuseria, M. A. Robb, J. R. Cheeseman, G. Scalmani, V. Barone, G. A. Petersson, H. Nakatsuji, X. Li, M. Caricato, A. V. Marenich, J. Bloino, B. G. Janesko, R. Gomperts, B. Mennucci, H. P. Hratchian, J. V. Ortiz, A. F. Izmaylov, J. L. Sonnenberg, D. Williams-Young, F. Ding, F. Lipparini, F. Egidi, J. Goings, B. Peng, A. Petrone, T. Henderson, D. Ranasinghe, V. G. Zakrzewski, J. Gao, N. Rega, G. Zheng, W. Liang, M. Hada, M. Ehara, K. Toyota, R. Fukuda, J. Hasegawa, M. Ishida, T. Nakajima, Y. Honda, O. Kitao, H. Nakai, T. Vreven, K. Throssell, J. J. A. Montgomery, J. E. Peralta, F. Ogliaro, M. J. Bearpark, J. J. Heyd, E. N. Brothers, K. N. Kudin, V. N. Staroverov, T. A. Keith, R. Kobayashi, J. Normand, K. Raghavachari, A. P. Rendell, J. C. Burant, S. S. Iyengar, J. Tomasi, M. Cossi, J. M. Millam, M. Klene, C. Adamo, R. Cammi, J. W. Ochterski, R. L. Martin, K. Morokuma, O. Farkas, J. B. Foresman, D. J. Fox, Gaussian 16 Revision C.01, **2016**, Gaussian Inc., Wallingford.
[36] J. E. D. Glendening, K. Badenhoop, A. E. Reed, J. E. Carpenter, J. A. Bohmann, C. M. Morales, P. Karafiloglou, C. R. Landis, F. Weinhold, NBO 7.0, **2018**, Theoretical Chemistry Institute, University of Wisconsin, Madison.
[37] C. Riplinger, P. Pinski, U. Becker, E. F. Valeev, F. Neese, *J. Chem. Phys.* **2016**, *144*.
[38] a) F. Neese, *WIREs Comput. Mol. Sci.* **2012**, *2*, 73–78; b) F. Neese, *WIREs Comput. Mol. Sci.* **2022**, *12*, e1606.
[39] S. R. Kirk, S. Jenkins, *WIREs Comput. Mol. Sci.* **2022**, *12*, e1611.
[40] A. K. Todd, *AIMAll (Version 19.10.12), TK Gristmill Software, Overland Park KS, USA, 2019 (aim.tkgristmill.com)*.
[41] a) B. Roberto, P. Francesca, L. Rubén, Q. Chaoyu, C. Alessandra, P. Jean-Philip, M. Yvon, C.-G. Julia, *NCIPLOT4: A New Step Towards a Fast Quantification of Noncovalent Interactions.* ChemRxiv. Cambridge: Cambridge Open Engage; **2019**; b) R. Laplaza, F. Peccati, R. A. Boto, C. Quan, A. Carbone, J.-P. Piquemal, Y. Maday, J. Contreras-García, *WIREs Comput. Mol. Sci.* **2021**, *11*, e1497.
[42] a) Z. Shuai, J. L. Brédas, *Phys. Rev. B* **1992**, *46*, 16135–16141; b) A. Guillén-López, C. Delesma, C. Amador-Bedolla, M. Robles, J. Muñiz, *Theor. Chem. Acc.* **2018**, *137*, 85; c) L.-j. Gong, C. Ma, C.-p. Li, J.-k. Lv, X.-y. Zhang, *New J. Chem.* **2020**, *44*, 10484–10491.
[43] a) K. He, N. Chen, C. Wang, L. Wei, J. Chen, *Cryst. Res. Technol.* **2018**, *53*, 1700157; b) E. A. Ekimov, O. S. Kudryavtsev, N. E. Mordvinova, O. I. Lebedev, I. I. Vlasov, *ChemNanoMat* **2018**, *4*, 269–273; c) M. K. Singh, A. Singh, in *Characterization of Polymers and Fibres* (Eds.: M. K. Singh, A. Singh), Woodhead Publishing, **2022**, pp. 153–185; d) S. Nasiri, M. Rabiei, A. Palevicius, G. Janusas, A. Vilkauskas, V. Nutalapati, A. Monshi, *Nano Trends* **2023**, *3*, 100015.
[44] a) R. K. Harris, E. D. Becker, S. M. C. d. Menezes, R. Goodfellow, P. Granger, *Pure Appl. Chem.* **2001**, *73*, 1795–1818; b) R. K. Harris, E. D. Becker, S. M. C. d. Menezes, P. Granger, R. E. Hoffman, K. W. Zilm, *Pure Appl. Chem.* **2008**, *80*, 59–84.
[45] A. E. Bennett, C. M. Rienstra, M. Auger, K. V. Lakshmi, R. G. Griffin, *J. Chem. Phys.* **1995**, *103*, 6951–6958.
[46] D. Jardón-Álvarez, J. Schmedt auf der Günne, *Solid State Nucl. Magn. Reson.* **2018**, *94*, 26–30.
[47] a) M. Bak, J. T. Rasmussen, N. C. Nielsen, *J. Magn. Reson.* **2000**, *147*, 296–330; b) Z. Tošner, R. Andersen, B. Stevensson, M. Edén, N. C. Nielsen, T. Vosegaard, *J. Magn. Reson.* **2014**, *246*, 79–93.

Manuscript received: March 8, 2024
Revised manuscript received: March 23, 2024
Accepted manuscript online: March 24, 2024
Version of record online: April 22, 2024